nature COMMUNICATIONS

ARTICLE

https://doi.org/10.1038/s41467-019-08784-z OPEN

Giant thermoelectric power factor in ultrathin FeSe superconductor

Sunao Shimizu[1], Junichi Shiogai[2], Nayuta Takemori[1], Shiro Sakai[1], Hiroaki Ikeda[3], Ryotaro Arita[1], Tsutomu Nojima[2], Atsushi Tsukazaki[2] & Yoshihiro Iwasa[1,4]

The thermoelectric effect is attracting a renewed interest as a concept for energy harvesting technologies. Nanomaterials have been considered a key to realize efficient thermoelectric conversions owing to the low dimensional charge and phonon transports. In this regard, recently emerging two-dimensional materials could be promising candidates with novel thermoelectric functionalities. Here we report that FeSe ultrathin films, a high-T_c superconductor (T_c; superconducting transition temperature), exhibit superior thermoelectric responses. With decreasing thickness d, the electrical conductivity increases accompanying the emergence of high-T_c superconductivity; unexpectedly, the Seebeck coefficient α shows a concomitant increase as a result of the appearance of two-dimensional natures. When d is reduced down to ~1 nm, the thermoelectric power factor at 50 K and room temperature reach unprecedented values as high as 13,000 and 260 μW cm^{-1} K^{-2}, respectively. The large thermoelectric effect in high T_c superconductors indicates the high potential of two-dimensional layered materials towards multi-functionalization.

[1] RIKEN Center for Emergent Matter Science (CEMS), Wako, Saitama 351-0198, Japan. [2] Institute for Materials Research, Tohoku University, Sendai 980-8577, Japan. [3] Department of Physics, Ritsumeikan University, Kusatsu, Shiga 525-8577, Japan. [4] Quantum Phase Electronics Center (QPEC) and Department of Applied Physics, University of Tokyo, Bunkyo, Tokyo 113-8656, Japan. These authors contributed equally: Sunao Shimizu, Junichi Shiogai. Correspondence and requests for materials should be addressed to Y.I. (email: iwasa@ap.t.u-tokyo.co.jp)

Two-dimensional (2D) materials are expanding their arena in terms of richness in material type, properties, and functions, which range from electronic devices to catalysts and medicines[1,2]. Thermoelectric generation is one of the physical functions in which 2D materials are anticipated to be superior in comparison with their bulk counterparts. The density of states (DOS) in 2D semiconductors is considerably different from that of three-dimensional (3D) materials at the band edge singularity[3]. As the Seebeck coefficient α is related to the profile of the DOS at the Fermi energy, 2D or low dimensional structures are considered to be advantageous for enhancing thermoelectric performance. Such a concept was proposed originally for semiconductor quantum wells and superlattices;[4] however, recently emerging 2D-layered materials provide naturally formed atomic layers and their hetero-structures[5], which are an ideal platform to elicit their intrinsic 2D nature. For characterization of thermoelectric properties of nanomaterials, on-chip device measurements have been often utilized[6–8]. Although the device configuration used for the measurements is not directly adapted to practical applications, it is highly powerful for realizing ideal conditions including the structures free from significant disorder and the tunable carrier density and thus for elucidating the intrinsic performance of materials. This method also fits the thermoelectric characterization of 2D materials in the present study.

The performance of thermoelectric semiconductors is measured by the figure of merit $ZT = \alpha^2 T/\rho\kappa$ (where ρ is the electrical resistivity, κ is the thermal conductivity, and T is the absolute temperature). Therefore, materials with the large power factor α^2/ρ can be candidates for high ZT. In order to maximize α^2/ρ, we propose to extensively investigate recent 2D layered materials. In addition to the possible enhancement of the Seebeck effect in 2D DOS, an important characteristic of the recent 2D materials is their excellent crystallinity, which is preferable for keeping a large conductivity even in nano-thick monolayers.

For our purpose, 3d transition-metal-based compounds should be more favorable than 4d and 5d counterparts because the wave functions of 3d-based compounds are more localized, generally causing a larger effective mass m^* and thus the larger DOS. Among 3d-based materials, we chose FeSe, first because a relatively large m^* ranging from 2 to 4 m_e has been reported in heavily electron-doped regions[9,10], where m_e is the free electron mass. The physical properties of ultrathin FeSe have attracted much attention because of the appearance of the unexpected high-T_c superconducting phase by reducing the film thickness down to a monolayer, the T_c of which reaches 65 K[11,12] or 100 K[13]. Surprisingly, the high conductivity value survives even in monolayer FeSe;[11,14,15] this is in stark contrast to conventional semiconductor thin films, where the resistance increases with reducing the thickness.

Here we report simultaneous measurements of α and ρ while controlling the thickness d of FeSe films on $SrTiO_3$ (001) substrates in an electric double-layer transistor configuration[16]. In previous studies, we succeeded in optimization of α^2/ρ with controlling n through the gate bias V_G and applied this technique to various materials[16] (see Methods). When V_G is applied at ~220 K, which is just above the glass transition temperature of the ionic liquid used in this study (see Methods), the cations or anions are self-aligned on the surface of FeSe; thus, charge carriers are electrostatically accumulated to form the electric double layer[17,18]. On the other hand, when a certain level of V_G is applied at higher temperatures such as ~245 K or above, an electrochemical reaction takes place at the liquid–solid interface, and the topmost FeSe layer dissolves into the ionic liquid in a pseudo layer-by-layer manner[15]. Therefore, systematic investigation of the thermoelectric properties from bulk to ultrathin FeSe now becomes possible at a wide temperature range from 10 K to around room temperature. We found that the thermoelectric effect is dramatically enhanced with reducing d down to ~1 nm and thermoelectric power factor at 50 K and room temperature reach unprecedented values as high as 13,000 and 260 μW cm^{-1} K^{-2}, respectively. The coexistence of giant thermoelectric power factor and high-T_c superconductivity indicates the high potential of 2D layered materials towards multi-functionalization.

Results

Electrochemically enhanced Seebeck effect in FeSe thin film. Dimensionality is a possible key factor to induce the evolution of the thermoelectric response owing to the characteristic DOS (Fig. 1a, b). The electric double layer transistor configuration shown in Fig. 1c enables us to control the film thickness d through the electrochemical etching on the surface of the FeSe films (Fig. 1d). Figure 2a shows the thermoelectric voltage ΔV as a

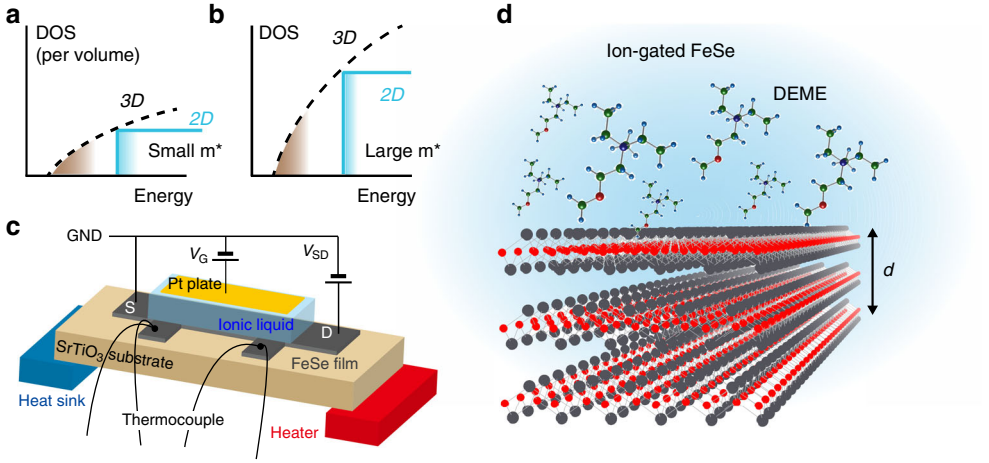

Fig. 1 Schematic device structure for thermoelectric measurement. **a** Schematic illustration of the electronic density of states (DOS) for three-dimensional (3D) and two-dimensional (2D) electrons. **b** The large effective mass m^* enhances the DOS, which is favorable to the enhancement of the Seebeck effect. **c** Device structure for thermoelectric measurement. V_{SD} and V_G stand for the source (S)—drain (D) voltage and the gate bias voltage, respectively. When V_G is applied to the Pt plate, ions in the ionic liquid are redistributed, forming an electric double layer on the surface of the FeSe film. **d** Enlarged illustration of the ionic liquid/FeSe interface. Under the positive gate bias, *N*,*N*-diethyl-*N*-(2-methoxyethyl)-*N*-methylammonium cations, DEME +, align on the surface of FeSe. The thickness d of the FeSe thin film was tuned by electrochemical etching[15]. See Methods for details of the device structure and fabrication

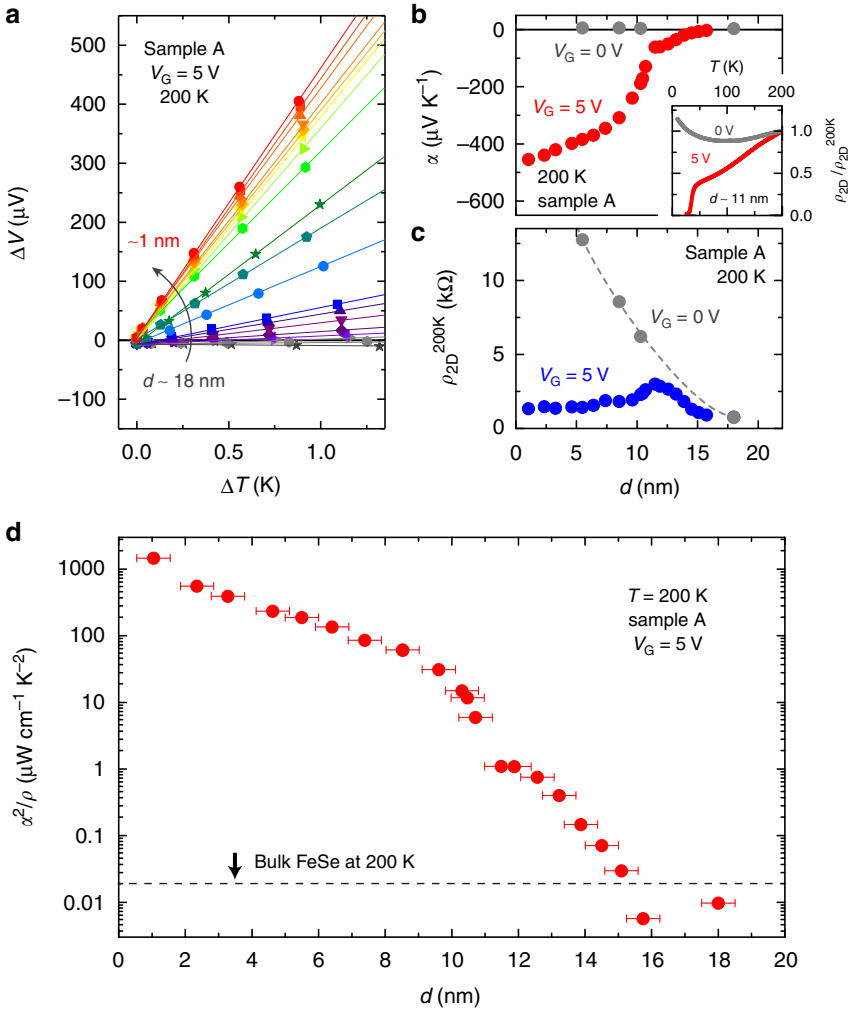

Fig. 2 Thinning-induced enhancement of thermoelectric effect. **a** Thermoelectric voltage ΔV under temperature difference ΔT in an FeSe thin film, Sample A. The thermoelectric measurements were performed at 200 K with $V_G = 5$ V. The value of ΔV changed its sign and dramatically increased with decreasing thickness d from ~18 nm to ~1 nm. **b** Thickness d dependence of the Seebeck coefficient α. The values of α were estimated from the slope of the $\Delta V - \Delta T$ plot in **a** as $\alpha = -\Delta V/\Delta T$. The inset shows the temperature T dependence of the normalized sheet resistance ρ_{2D} with respect to 200 K. Superconductivity appeared when $V_G = 5$ V was applied. **c** Variation of sheet resistance $\rho_{2D}{}^{200\,K}$ at 200 K as a function of d. The value of $\rho_{2D}{}^{200\,K}$ for $V_G =$ 5 V showed a weak d dependence (blue circles), whereas that for $V_G = 0$ V increased with decreasing d (gray circles). **d** Thickness d dependence of thermoelectric power factor α^2/ρ exhibiting anomalous enhancement in the ultrathin limit. Here, ρ is the electrical resistivity, which is estimated as $\rho = \rho_{2D} \times d$. The value of α^2/ρ at 200 K in the thick region is comparable to that in bulk FeSe[19], whereas α^2/ρ increased with decreasing d because of the double-digit increase of α in ultrathin regions in **b**. The error bar of d corresponds to ~ ± 0.5 nm, which was estimated from the surface roughness of the initial thin film[15]

function of the temperature difference ΔT between two thermocouples (see Fig. 1c) in Sample A at $V_G = 5$ V. Here, it is noted that the application of V_G not only induces the electrochemical etching of the thin films but also accumulates the electron carriers on the top surface. The thermoelectric measurement was done at 200 K; possible conduction paths through the ionic liquid are completely eliminated. The device was cooled down to 200 K for the measurement at each thickness d after electrochemical etching at higher temperatures[15]. All the ΔV plots for different d's linearly depended on ΔT, securing the accurate characterization of the Seebeck effect. At 200 K, ΔV was dramatically enhanced across the sign change with decreasing d from ~18 nm to ~1 nm. Figure 2b plots the d dependence of α ($= -\Delta V/\Delta T$) at 200 K for $V_G = 5$ V. A very small α of $+3.8\,\mu V\,K^{-1}$ at d ~18 nm is consistent with the reported values on bulk FeSe[19,20], where such a small α value reflects the semimetallic electronic structure[21]. With the thickness reduction, on the other hand, the absolute value of α was surprisingly enhanced by two orders of magnitude up to $|-454\,\mu V\,K^{-1}|$.

It should be noted that the parasitic conduction of the $SrTiO_3$ substrate is ruled out because the gate electric field on $SrTiO_3$ through the FeSe thin films is negligible in the present configuration owing to the screening effect in the metallic conducting FeSe and also the formation of the Schottky barrier at the FeSe/$SrTiO_3$ interface[22–24] (see Supplementary Figure 1, Supplementary Figure 2, and Supplementary Note 1). The existence of an oxygen deficient layer at the surface of $SrTiO_3$ substrate as a source of the large Seebeck response is also definitely ruled out as the large α is observed only under gate bias and is suppressed to bulk-like small values by switching off V_G to 0 V, as seen in the main panel of Fig. 2b. Importantly, the high-T_c superconductivity appears by applying $V_G = 5$ V and disappears by removing V_G[15,17,18], as shown in the inset of Fig. 2b. The simultaneous emergence of the giant thermoelectric response and

the high-T_c superconductivity proves that these two transport properties arise from the same electronic state of FeSe thin films.

Another noticeable feature of FeSe thin films is the low electrical resistance realized even in ultrathin regions. Figure 2c shows the 2D sheet resistance ρ_{2D} of Sample A for $V_G = 0$ V (gray circles) and 5 V (blue circles) as a function of d. When starting from the initial state with d ~18 nm, the sheet resistance at 200 K, $\rho_{2D}^{200\,K}$, first increased with decreasing d for both $V_G = 0$ V and 5 V. With further decreasing d, $\rho_{2D}^{200\,K}$ at $V_G = 5$ V showed a small peak at around d ~11 nm and kept small values down to d ~1 nm because the gated topmost layer of FeSe and the charge transfer layer at the FeSe/$SrTiO_3$ interface dominate the electrical transport of the thin film (see Supplementary Figure 3 and Supplementary Note 2 for the details of the d dependence of $\rho_{2D}^{200\,K}$). Such a low electrical resistance irrespective of the film thickness is consistent with the previous studies; for example, the resistivity of monolayer or few layer MBE-grown FeSe[11,14] is comparable to that of 10 nm thick (~15 layers) FeSe[17,18] owing to the interface or surface electron doping. Actually, $\rho_{2D}^{200\,K}$ ~1 kΩ at $V_G = 5$ V in the thin limit (Fig. 2c) is close to that in doped FeSe monolayers[11,14,15]. On the other hand, the small α and high $\rho_{2D}^{200\,K}$ at $V_G = 0$ V indicate that the charge transfer layer does not produce the enhanced values of α. Consequently, the thermoelectric power factor α^2/ρ at 200 K achieved a dramatic development in Fig. 2d owing to the enhancement of α and the concomitant reduction of electrical resistivity $\rho = \rho_{2D} \times d$, which rarely occurs in the framework of conventional material design and fabrication. Along with the reduction of d from 18 nm to 1 nm, α^2/ρ kept increasing and finally reached ~1500 μW $cm^{-1}K^{-2}$.

Temperature-thickness mapping of thermoelectric response. Figures 3a, b display the temperature T—thickness d mappings of the absolute value of α (i.e., $|\alpha|$) and α^2/ρ, respectively, for another FeSe thin film, Sample B. The values of $|\alpha|$ and α^2/ρ showed dramatic developments in the nanometer-thick region, which agrees well with the results for Sample A (see Figs. 2b, c). Moreover, the enhancement for both $|\alpha|$ and α^2/ρ covers a wide temperature range from 50 K (just above T_c) to 280 K. Figure 3c summarizes α^2/ρ for representative thermoelectric materials that possess high α^2/ρ values (see Supplementary Table 1). The values of α^2/ρ for the FeSe ultrathin film increased from ~260 μW cm^{-1} K^{-2} at 280 K up to ~13,000 μW cm^{-1} K^{-2} at 50 K, being the largest among existing bulk materials reported so far. Assuming the thermal conductivity for bulk Fe-based superconductors[25,26], κ ~5 W m^{-1} K^{-1}, the dimensionless figure of merit ZT of the FeSe ultrathin film reaches as large as ~1.5 at 280 K.

Common trend of Seebeck effect in Fe-based superconductors. The detailed temperature dependence of α for different d's is presented in Fig. 4a to show the unusual thermoelectric response in FeSe. Except for the initial thickness (19.1 nm) with moderate

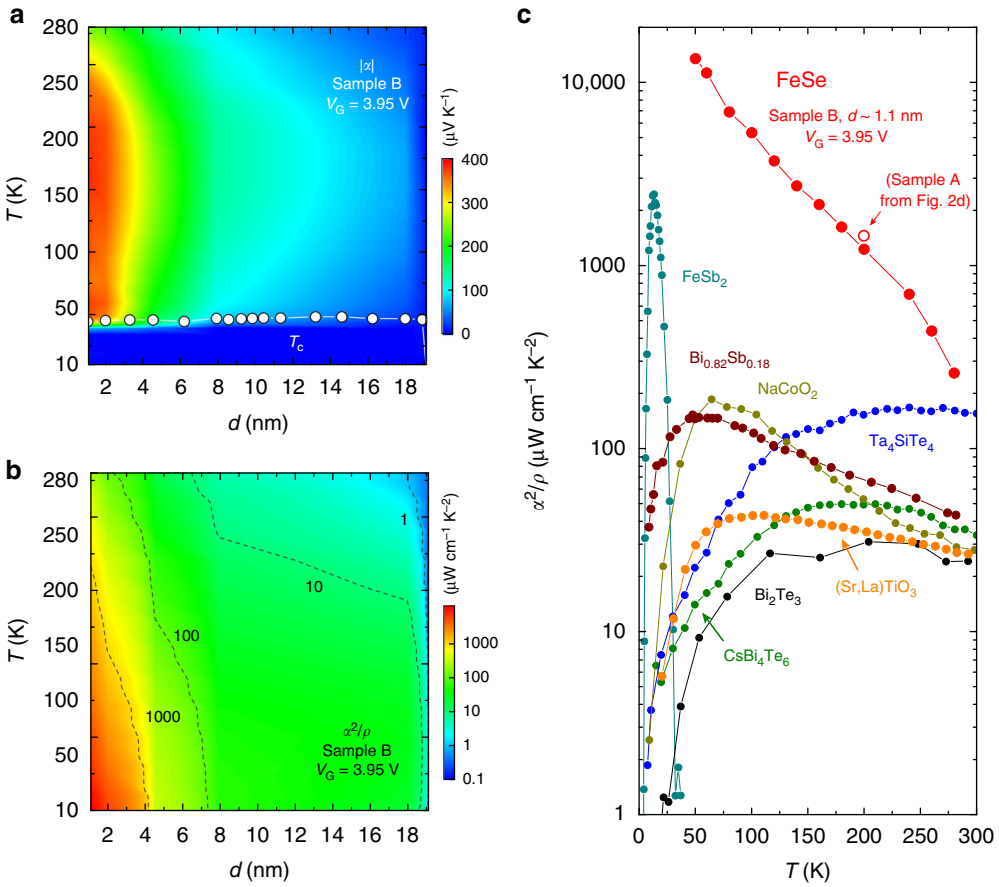

Fig. 3 Giant thermoelectric response in ultrathin FeSe. **a** Mapping of Seebeck coefficient α of FeSe (Sample B) against temperature T and thickness d. Here, the absolute value of α (i.e., $|\alpha|$) for $V_G = 3.95$ V was plotted. The white circles correspond to the onset temperature T_c of the superconducting transition. **b** Evolution of thermoelectric power factor α^2/ρ of FeSe (Sample B) above T_c. The value of α^2/ρ increased with decreasing d, mainly owing to the large enhancement of α shown in **a**. **c** Comparison of temperature dependence of α^2/ρ among representative thermoelectric materials. The values of α^2/ρ in the FeSe ultrathin film were larger than any existing bulk materials reported so far in a wide temperature range (see Supplementary Table 1 for the reference of the experimental values). The data point for Sample A at 200 K (open circle) shows fair reproducibility

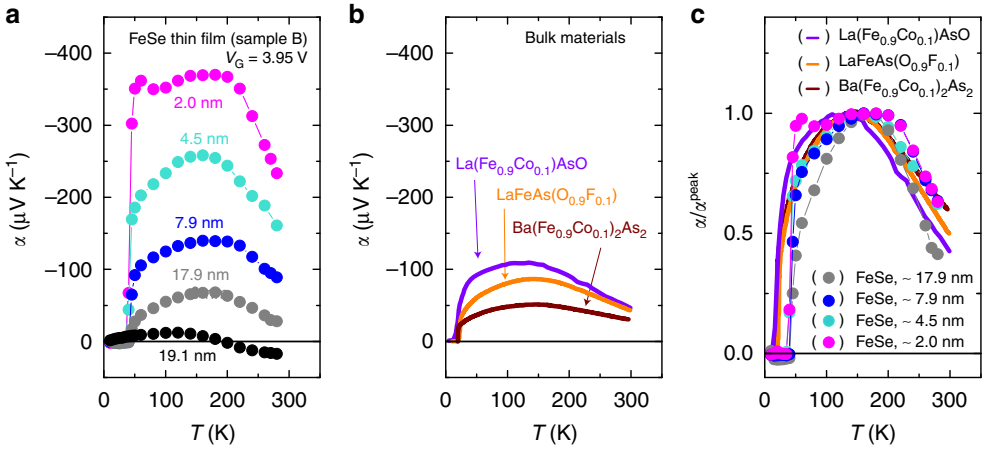

Fig. 4 Temperature dependence of Seebeck coefficient. **a** Seebeck coefficient α vs. temperature T in FeSe thin film (Sample B). The values of α were enhanced by the thickness reduction in all temperature regions. **b** $\alpha-T$ curves in representative Fe-based high-T_c superconductors. $Ba(Fe_{0.9}Co_{0.1})_2As_2$[27], $LaFeAs(O_{0.9}F_{0.1})$[28], and $La(Fe_{0.9}Co_{0.1})AsO$[29] show the peak behavior at ~150 K, in a similar manner to the FeSe thin film in **a**. **c** Temperature dependence of α normalized by the peak value α^{peak} for FeSe thin films and bulk materials in **b**. Overall temperature variation of α is seemingly common for Fe-based superconductors

temperature dependence, α for Sample B showed a peak at around ~200 K, which follows neither the T-linear behavior expected in conventional metals nor the phonon drag thermopower (see Supplementary Figure 1 and Supplementary Note 1). Actually, the temperature dependence of α in the FeSe thin film is qualitatively similar to that in bulk Fe-based high-T_c superconductors such as $Ba(Fe_{0.9}Co_{0.1})_2As_2$[27], $LaFeAs(O_{0.9}F_{0.1})$[28], and $La(Fe_{0.9}Co_{0.1})AsO$[29], as shown in Fig. 4b. This trend can be seen even more clearly in Fig. 4c, where the data in Fig. 4a, b are normalized by the peak value α^{peak} of each sample. These similarities further prove that α observed in Fig. 4a is attributed to FeSe itself rather than other artifacts such as substrates and ionic liquids. The characteristic temperature dependence of α/α^{peak} in Fig. 4c is considered unique to Fe-based superconductors and has been discussed in the context of quantum criticality[30–32] or the two carrier model[27,33]. For example, it was reported that $|\alpha|/T$ in $Ba(Fe_{0.9}Co_{0.1})_2As_2$[27] shows a divergence above T_c and a strong enhancement when in proximity to the quantum critical point.

Electronic band structure in gated FeSe thin film. The transfer characteristics (the V_G dependence of resistance) of a FeSe thin film (see Supplementary Figure 4 and Supplementary Note 3) indicates that the dominant carriers change from holes to electrons with reducing the thickness. This behavior is consistent with the band structure evolution derived from the angle-resolved photoemission spectroscopy (ARPES)[12,34–36] in monolayer FeSe on $SrTiO_3$ and in K-coated FeSe thin films, which clarified that the hole pocket at the Γ-point disappears and a gap of ~60 meV is opened at the M-point[34] owing to the thinning and concomitant electron doping. The present ion-gated FeSe thin films should have a similar band structure because the electron density accumulated by the ionic gating, ~10^{14} cm^{-2}, is comparable to that of the charge transfer from $SrTiO_3$ substrate and of surface K coating. This band structure of FeSe monolayer should be beneficial for the enhancement of $|\alpha|$. We calculated the Seebeck coefficient for the undoped bulk FeSe and electron-doped monolayer FeSe at $T = 280$ K (see Supplementary Figure 5 and Supplementary Note 4), and obtained α values as $+5$ μV K^{-1} and -200 μV K^{-1} for the bulk and the monolayer FeSe, respectively. These estimations reasonably explain the experimental values of α at 280 K: $+17$ μV K^{-1} and -245 μV K^{-1} (Fig. 3a) for the initial (d ~19.1 nm) and final (d ~1 nm) thicknesses, respectively. On the other hand, our calculation based on the Fermi liquid picture predicts T-linear behavior and does not explain the non-monotonous temperature dependence of α in ultrathin FeSe. The experimentally observed broad peak in α located at ~200 K (Fig. 4a) is suggestive of a crucial role of electronic correlations in the Seebeck response of ultrathin FeSe; in fact, the recent ARPES studies pointed out a strong electronic correlation[9] in the high-T_c phase of FeSe. A quantitative theoretical analysis of this effect remains to be performed.

Discussion

Nanostructures or low-dimensional structures have been a powerful guideline for the exploration of high-performance thermoelectric materials[8,37–40]. The present results show that further enhancement of thermoelectric properties should be possible, if peculiar band structures of nano-structured systems including 2D layered materials are combined with additional ingredients such as strong electronic correlations. The unprecedented coexistence of giant thermoelectric power factor and high-T_c superconductivity in ultrathin FeSe exemplifies that there may exist unknown multifunctional materials waiting to be disclosed in extreme conditions, illuminating a next research direction of functional thermoelectric materials.

Methods

Device fabrication. We fabricated ion-gated devices based on FeSe-thin films on $SrTiO_3$ substrates[15] with channel size of 1.2×2 mm^2. The details of the thin-film preparation were reported in our previous study[15]. The device structure used in this study is schematically shown in Fig. 1c. The FeSe thin films were patterned by using a laser cutter to perform four-terminal resistance measurements. The gold wires were attached at both edges of the patterned film, working as a drain terminal D and a source terminal S. An ionic liquid, which worked as a gate dielectric, was placed on the FeSe surface. We used *N*,*N*-diethyl-*N*-(2-methoxyethyl)-*N*-methylammonium bis-(trifluoromethylsulfonyl)-imide (DEME-TFSI) as the ionic liquid. A Pt plate was placed on top of them, working as a gate electrode.

Thermoelectric measurements under gate biases. As shown in Fig. 1c, a heater and a heat sink were attached to either side of the ion-gated device to produce a thermal gradient. The type E thermocouples were attached to monitor the temperature difference ΔT and the thermoelectric voltage ΔV. The thermocouples were also used for the four-terminal resistance measurements. The temperature difference ΔT (0–1 K) and the voltage ΔV between the thermocouples were measured, and the values of α were evaluated from the slope of the $\Delta V-\Delta T$ plots (See Fig. 2a). This device configuration allows us to measure α and ρ simultaneously. The thermoelectric measurements with solid[41–47] and ionic gate dielectrics[48–57] are widely accepted as a method to evaluate the thermoelectric properties of semiconductors with changing the carrier densities.

Calculations. We performed first-principles band structure calculations using the Perdew-Burke-Ernzerhof parameterization of the generalized gradient approximation[58] and the full-potential (linearized) augmented plane-wave method, with the inclusion of spin-orbit coupling as implemented in the wien2k code[59]. Muffin-tin radii (R_{MT}) of 2.38 and 2.11 Bohr were used for Fe and Se, respectively. The maximum modulus for the reciprocal vectors K_{max} was chosen such that $R_{MT}K_{max} = 7.0$ and a $10 \times 10 \times 10$ k-mesh in the first Brillouin zone was used. The tight-binding Hamiltonian for the *3d* orbitals of the Fe atom was constructed with Wannier90[60] and wien2wannier[61].

Data availability

The authors declare that all data supporting the findings of this study are available within the paper and its Supplementary Information or from the authors upon reasonable request.

Received: 5 August 2018 Accepted: 25 January 2019
Published online: 18 February 2019

References

1. Fiori, G. et al. Electronics based on two-dimensional materials. *Nat. Nanotechnol.* **9**, 768–779 (2014).
2. Chhowalla, M. et al. The chemistry of two-dimensional layered transition metal dichalcogenide nanosheets. *Nat. Chem.* **5**, 263–275 (2013).
3. Dresselhaus, M. S. et al. New directions for low-dimensional thermoelectric materials. *Adv. Mater.* **19**, 1043–1053 (2007).
4. Hicks, L. D. & Dresselhaus, M. S. Effect of quantum-well structures on the thermoelectric figure of merit. *Phys. Rev. B* **47**, 12727–12731 (1993).
5. Geim, A. K. & Grigorieva, I. V. Van der Waals heterostructures. *Nature* **499**, 419–425 (2013).
6. Venkatasubramanian, R., Siivola, E., Colpitts, T. & O'Quinn, B. Thin-film thermoelectric devices with high room-temperature figures of merit. *Nature* **413**, 597–602 (2001).
7. Harman, T. C., Taylor, P. J., Walsh, M. P. & La Forge, B. E. Quantum dot superlattice thermoelectric materials and devices. *Science* **297**, 2229–2232 (2002).
8. Ohta, H. et al. Giant thermoelectric Seebeck coefficient of a two-dimensional electron gas in $SrTiO_3$. *Nat. Mater.* **6**, 129–134 (2007).
9. Wen, C. H. P. et al. Anomalous correlation effects and unique phase diagram of electron-doped FeSe revealed by photoemission spectroscopy. *Nat. Commun.* **7**, 10840 (2016).
10. Seo, J. J. et al. Superconductivity below 20 K in heavily electron-doped surface layer of FeSe bulk crystal. *Nat. Commun.* **7**, 11116 (2016).
11. Wang, Q.-Y. et al. Interface-induced high-temperature superconductivity in single unit-cell FeSe films on $SrTiO_3$. *Chin. Phys. Lett.* **29**, 037402 (2012).
12. Liu, D. et al. Electronic origin of high-temperature superconductivity in single-layer FeSe superconductor. *Nat. Commun.* **3**, 931 (2012).
13. Ge, J.-F. et al. Superconductivity above 100 K in single-layer FeSe films on doped $SrTiO_3$. *Nat. Mater.* **14**, 285–289 (2014).
14. Sun, Y. et al. High temperature superconducting FeSe films on $SrTiO_3$ substrates. *Sci. Rep.* **4**, 6040 (2014).
15. Shiogai, J., Ito, Y., Mitsuhashi, T., Nojima, T. & Tsukazaki, A. Electric-field-induced superconductivity in electrochemically etched ultrathin FeSe films on $SrTiO_3$ and MgO. *Nat. Phys.* **12**, 42–46 (2016).
16. Bisri, S. Z., Shimizu, S., Nakano, M. & Iwasa, Y. Endeavor of iontronics: from fundamentals to applications of ion-controlled Electronics. *Adv. Mater.* **29**, 1607054 (2017).
17. Lei, B. et al. Evolution of high-temperature superconductivity from a low T_c phase tuned by carrier concentration in FeSe thin Flakes. *Phys. Rev. Lett.* **116**, 077002 (2016).
18. Hanzawa, K., Sato, H., Hiramatsu, H., Kamiya, T. & Hosono, H. Electric field-induced superconducting transition of insulating FeSe thin film at 35 K. *Proc. Natl. Acad. Sci. USA* **113**, 3986–3990 (2016).
19. McQueen, T. M. et al. Extreme sensitivity of superconductivity to stoichiometry in $Fe_{1+\delta}Se$. *Phys. Rev. B* **79**, 014522 (2009).
20. Song, Y. J. et al. Superconducting properties of a stoichiometric FeSe compound and two anomalous features in the normal State. *J. Korean Phys. Soc.* **59**, 312–316 (2011).
21. Nakayama, K. et al. Reconstruction of band structure induced by electronic nematicity in an FeSe superconductor. *Phys. Rev. Lett.* **113**, 237001 (2014).
22. Wu, C. T. et al. Heterojunction of $Fe(Se_{1-x}Te_x)$ superconductor on Nb-doped $SrTiO_3$. *Appl. Phys. Lett.* **96**, 122506 (2010).
23. Zhang, W. et al. Interface charge doping effects on superconductivity of single-unit-cell FeSe films on $SrTiO_3$ substrates. *Phys. Rev. B* **89**, 060506(R) (2014).
24. Zhang, H. et al. Origin of charge transfer and enhanced electron-phonon coupling in single unit-cell FeSe films on $SrTiO_3$. *Nat. Commun.* **8**, 214 (2017).
25. Machida, Y. et al. Possible sign-reversing s-wave superconductivity in co-doped $BaFe_2As_2$ proved by thermal transport measurements. *J. Phys. Soc. Jpn.* **78**, 073705 (2009).
26. Checkelsky, J. G. et al. Thermal hall conductivity as a probe of gap structure in multiband superconductors: the case of $Ba_{1-x}KxFe_2As_2$. *Phys. Rev. B* **86**, 180502(R) (2012).
27. Arsenijević, S. et al. Pressure effects on the transport coefficients of $Ba(Fe_{1-x}Co_x)_2As_2$. *Phys. Rev. B* **84**, 075148 (2011).
28. Zhu, Z. W. et al. Nernst effect of a new iron-based superconductor $LaO_{1-x}F_xFeAs$. *New J. Phys.* **10**, 063021 (2008).
29. Kondrat, A., Behr, G., Büchner, B. & Hess, C. Unusual Nernst effect and spin density wave precursors in superconducting $LaFeAsO_{1-x}F_x$. *Phys. Rev. B* **83**, 092507 (2011).
30. Gooch, M., Lv, B., Lorenz, B., Guloy, A. M. & Chu, C. W. Critical scaling of transport properties in the phase diagram of iron pnictide superconductors $K_xSr_{1-x}Fe_2As_2$ and $K_xBa_{1-x}Fe_2As_2$. *J. Appl. Phys.* **107**, 09E145 (2010).
31. Maiwald, J., Jeevan, H. S. & Gegenwart, P. Signatures of quantum criticality in hole-doped and chemically pressurized $EuFe_2As_2$ single crystals. *Phys. Rev. B* **85**, 024511 (2012).
32. Arsenijević, S. et al. Signatures of quantum criticality in the thermopower of $Ba(Fe_{1-x}Co_x)_2As_2$. *Phys. Rev. B* **87**, 224508 (2013).
33. Sales, B. C., McGuire, M. A., Sefat, A. S. & Mandrus, D. A semimetal model of the normal state magnetic susceptibility and transport properties of $Ba(Fe_{1-x}Co_x)_2As_2$. *Phys. C.* **470**, 304–308 (2010).
34. He, S. et al. Phase diagram and electronic indication of high-temperature superconductivity at 65 K in single-layer FeSe films. *Nat. Mater.* **12**, 605–610 (2013).
35. He, J. et al. Electronic evidence of an insulator-superconductor transition in single-layer $FeSe/SrTiO_3$ films. *Proc. Natl Acad. Sci. USA* **111**, 18501–18506 (2014).
36. Miyata, Y., Nakayama, K., Sugawara, K., Sato, T. & Takahashi, T. High-temperature superconductivity in potassium-coated multilayer FeSe thin films. *Nat. Mater.* **14**, 775–779 (2015).
37. Choi, W. S., Ohta, H., Moon, S. J., Lee, Y. S. & Noh, T. W. Dimensional crossover of polaron dynamics in $Nb:SrTiO_3/SrTiO_3$ superlattices: Possible mechanism of thermopower enhancement. *Phys. Rev. B* **82**, 024301 (2010).
38. Ohta, H. et al. Field-induced water electrolysis switches an oxide semiconductor from an insulator to a metal. *Nat. Commun.* **1**, 118 (2010).
39. Ohta, H. et al. Unusually large enhancement of thermopower in an electric field induced two-dimensional electron gas. *Adv. Mater.* **24**, 740–744 (2012).
40. Zhang, Y. et al. Double thermoelectric power factor of a 2D electron system. *Nat. Commun.* **9**, 2224 (2018).
41. Zavaritsky, N. V. Phonon drag in two-dimensional electron systems. *Phys. B +C.* **126**, 369–376 (1984).
42. Gallagher, B. L., Gibbings, C. J., Pepper, M. & Cantrell, D. G. The thermopower of Si inversion layers. *Semicond. Sci. Technol.* **2**, 456–459 (1987).
43. Small, J., Perez, K. & Kim, P. Modulation of thermoelectric power of individual carbon nanotubes. *Phys. Rev. Lett.* **91**, 256801 (2003).
44. Yoshikawa, A. et al. Electric-field modulation of thermopower for the $KTaO_3$ field-effect transistors. *Appl. Phys. Express* **2**, 121103 (2009).
45. Checkelsky, J. & Ong, N. Thermopower and Nernst effect in graphene in a magnetic field. *Phys. Rev. B* **80**, 081413 (2009).
46. Zuev, Y., Chang, W. & Kim, P. Thermoelectric and magnetothermoelectric transport measurements of graphene. *Phys. Rev. Lett.* **102**, 096807 (2009).
47. Ohta, H. et al. Field-modulated thermopower in $SrTiO_3$-based field-effect transistors with amorphous $12CaO \cdot 7Al_2O_3$ glass gate insulator. *Appl. Phys. Lett.* **95**, 113505 (2009).
48. Shimizu, S., Ono, S., Hatano, T., Iwasa, Y. & Tokura, Y. Enhanced cryogenic thermopower in $SrTiO_3$ by ionic gating. *Phys. Rev. B* **92**, 165304 (2015).
49. Yoshida, M. et al. Gate-optimized thermoelectric power factor in ultrathin WSe_2 single crystals. *Nano. Lett.* **16**, 2061–2065 (2016).
50. Shimizu, S. et al. Enhanced thermopower in ZnO two-dimensional electron gas. *Proc. Natl Acad. Sci. USA* **113**, 6438–6443 (2016).
51. Shimizu, S. et al. Thermoelectric detection of multi-subband density of states in semiconducting and metallic single-walled carbon nanotubes. *Small* **12**, 3388–3392 (2016).
52. Yanagi, K. et al. Tuning of the thermoelectric properties of one-dimensional materials networks by electric double layer techniques using ionic liquids. *Nano. Lett.* **14**, 6437 (2014).
53. Takayanagi, R., Fujii, T. & Asamitsu, A. Simultaneous control of thermoelectric properties in p- and n-type materials by electric double-layer gating: New design for thermoelectric device. *Appl. Phys. Express* **8**, 051101 (2015).
54. Chien, Y.-Y., Yuan, H. T., Wang, C.-R. & Lee, W.-L. Thermoelectric power in bilayer graphene device with ionic liquid gating. *Sci. Rep.* **6**, 20402 (2016).

55. Kawasugi, Y. et al. Simultaneous enhancement of conductivity and Seebeck coefficient in an organic Mott transistor. *Appl. Phys. Lett.* **109**, 233301 (2016).
56. Pu, J. et al. Enhanced thermoelectric power in two-dimensional transition metal dichalcogenide monolayers. *Phys. Rev. B* **94**, 014312 (2016).
57. Kawai, H. et al. Thermoelectric properties of WS_2 nanotube networks. *Appl. Phys. Express* **10**, 015001 (2017).
58. Perdew, J. P., Bruke, K. & Ernzerhof, M. Generalized gradient approximation made simple. *Phys. Rev. Lett.* **77**, 3865–3868 (1996).
59. Blaha, P., Schwarz, K., Madsen, G., Kvasnicka, D. & Luitz, J. *WIEN2k, An Augmented Plane Wave+Local Orbitals Program for Calculating Crystal Properties*. (Tech. Univ, Wien, 2001).
60. Mostofi, A. A. et al. wannier90: a tool for obtaining maximally-localised Wannier functions. *Comput. Phys. Commun.* **178**, 685–699 (2008).
61. Kuneš, J. et al. Wien2wannier: From linearized augmented plane waves to maximally localized Wannier functions. *Comput. Phys. Commun.* **181**, 1888–1895 (2010).

Acknowledgements

This work was supported by JSPS KAKENHI Grant Numbers JP25000003, JP16H00923 (SATL), JP16H06345, JP17H02928, JP17K19060.

Author contributions

S.Sh. and J.S. equally contributed to this work. S.Sh., J.S., T.N., A.T. and Y.I. conceived and designed this work. S.Sh., N.T., S.Sa., A.T. and Y.I. wrote the paper. S.Sh. and J.S. performed all the measurements, and N.T., S.Sa., H.I. and R.A. conducted the calculations. All authors contributed to discussions.

Additional information

Supplementary Information accompanies this paper at https://doi.org/10.1038/s41467-019-08784-z.

Competing interests: The authors declare no competing interests.

Reprints and permission information is available online at http://npg.nature.com/reprintsandpermissions/

Journal peer review information: *Nature Communications* thanks the anonymous reviewers for their contribution to the peer review of this work. Peer reviewer reports are available.

Publisher's note: Springer Nature remains neutral with regard to jurisdictional claims in published maps and institutional affiliations.